Biology of Reproduction, 2021, 104(5), 1022–1033
doi:10.1093/biolre/ioab021
Research Article
Advance Access Publication Date: 16 February 2021

Research Article

Conceptus metabolomic profiling reveals stage-specific phenotypes leading up to pregnancy recognition in cattle†

Constantine A. Simintiras[1,*], José M. Sánchez[1], Michael McDonald[1], Elena O'Callaghan[1], Ahmed A. Aburima[2] and Patrick Lonergan[1]

[1]School of Agriculture and Food Science, University College Dublin, Belfield, Dublin 4, Ireland and [2]Centre for Atherothrombotic and Metabolic Research, Hull York Medical School, Kingston-Upon-Hull, UK

***Correspondence:** Interdisciplinary Reproduction and Health Group, Division of Animal Sciences, University of Missouri, Columbia 65211, MO, USA. E-mail: c.simintiras@missouri.edu
†Grant Support: This work was supported by Science Foundation Ireland (13/IA/1983 PL), The Irish Research Council (GOIPD/2017/942 CAS), University College Dublin (CDA54580 CAS), and The British Heart Foundation (FS/19/10/34128 AAA).

Received 19 November 2020; Revised 16 January 2021; Accepted 3 February 2021

Abstract

Reproductive efficiency in livestock is a major driver of sustainable food production. The poorly understood process of ruminant conceptus elongation (a) prerequisites maternal pregnancy recognition, (b) is essential to successful pregnancy establishment, and (c) coincides with a period of significant conceptus mortality. Conceptuses at five key developmental stages between Days 8–16 were recovered and cultured in vitro for 6 h prior to conditioned media analysis by untargeted ultrahigh-performance liquid chromatography tandem mass spectroscopy. This global temporal biochemical interrogation of the ex situ bovine conceptus unearths two antithetical stage-specific metabolic phenotypes during tubular (metabolically retentive) vs. filamentous (secretory) development. Moreover, the retentive conceptus phenotype on Day 14 coincides with an established period of elevated metabolic density in the uterine fluid of heifers with high systemic progesterone—a model of accelerated conceptus elongation. These data, combined, suggest a metabolic mechanism underpinning conceptus elongation, thereby enhancing our understanding of the biochemical reciprocity of maternal–conceptus communication, prior to maternal pregnancy recognition.

Summary sentence

Temporal changes in conceptus metabolism occur in the period leading to maternal pregnancy recognition.

Key words: bovine, conceptus, development, elongation, embryo, metabolomics.

Introduction

The elongating ruminant conceptus (embryo and extra-embryonic tissues) undergoes (i) a morphological transition from spherical to ovoid to tubular to filamentous [1, 2], (ii) extraembryonic membrane differentiation [3], and (iii) a rapid increase in trophectoderm mass and length [4] around a seemingly randomly distributed axis [5]. The process of elongation is reproductively essential, not least as the concentration of the conceptus-derived signal required to trigger the maternal pregnancy recognition cascade, interferon tau (IFNT) [6, 7], is proportional to conceptus size [8]. Whilst a threshold concentration of IFNT required to establish pregnancy has yet to be established [9], the conceptus must first elongate to a sufficient length to establish pregnancy, with short conceptuses failing to elicit an appropriate response from the endometrium [10]. Only then can

apposition, attachment, adhesion, and full placentation commence [11].

Several studies into early (Days 1–7) bovine embryo metabolism, among other species, have led to a comprehensive understanding of the metabolic character of the early embryo; notably amino acid, glucose, lactate, and pyruvate utilization. Specifically, incremental modifications [12] to embryo culture media have unearthed the importance of several metabolites to early embryo development. However, the metabolic traits of the elongating conceptus remain poorly defined, partly owing to the technical constraints associated with obtaining conceptuses, as elongation has not, as yet, been recapitulated in vitro [13–15]. Indeed, this is an active area of research [16, 17].

The importance of optimal metabolism to successful conceptus elongation is apparent as (a) many genes expressed by the early elongating bovine conceptus relate to metabolism [18, 19], (b) a greater enrichment of differentially expressed genes relating to metabolism and biosynthesis has been observed in long vs. short (i.e., likely retarded) conceptuses [20, 21], and (c) conceptus elongation does not occur in vitro or in vivo in the absence of uterine glands [22]. Furthermore, exogenous systemic progesterone (P4) supplementation—a model which accelerates the rate of conceptus elongation [23]—results in select endometrial metabolite amplification in uterine lumen fluid (ULF) on Day 14 [24–27]. It is also worth noting that, to our knowledge, only one study has investigated ruminant conceptus metabolite consumption and release, in which the turnover of 18 amino acids by Days 14–16 bovine conceptuses cultured in vitro was quantified [28].

Given the importance of metabolism to conceptus development, in addition to the conceptus elongation window coinciding with a period of significant pregnancy loss in cattle [29–32], a better understanding of conceptus metabolism during this critical period in pregnancy establishment is essential. To this end, our aim was to comprehensively characterize the biochemical turnover of the bovine conceptus during the peri-elongation period (Days 8–16) using high-throughput untargeted ultra-high-performance liquid chromatography mass spectrometry. Our hypotheses were that (a) total metabolite uptake would increase with time—in line with likely elevated metabolic demands associated with exponential cellular proliferation, (b) metabolite consumption and secretion would correlate inversely to previously identified ULF metabolite turnover [24–27], and (c) the pattern of specific metabolite utilization would differ between the spherical vs. filamentous conceptus.

Materials and methods

Unless otherwise stated, all reagents were procured from Sigma Aldrich (Arklow, Ireland).

Experimental design

Bovine conceptuses at five developmental time-points leading up to maternal pregnancy recognition—Days 8, 10, 12, 14, and 16—were cultured in vitro for 6 h prior to the profiling of their conditioned media. To obtain Days 10–16 conceptuses, Day 7 in vitro produced blastocysts (Day 0 = day of in vitro fertilization) were transferred into synchronized heifers 8 days after the onset of estrus (Figure 1A); Day 8 embryos were obtained following an additional 24 h in in vitro culture. For consistency, the same volume of culture medium (500 µL per well) was used across all groups. To maximize the likelihood of metabolite detection in conceptus-conditioned culture media, smaller Days 8–14 conceptuses were cultured in groups, whereas Day 16 conceptuses were cultured individually (Figure 1B and C). Five biological replicates per developmental stage were carried out. Post-culture, conceptuses were recovered and analyzed for total protein content (Figure 1D and E), to enable metabolomic data normalization by total protein, in addition to per conceptus (discussed below).

Embryo production

In vitro maturation (IVM), fertilization (IVF), and culture (IVC) were performed to produce 373 grade 1 blastocysts, of which 305 were transferred into the recipient heifers. The remaining 68 blastocysts comprised the Day 8 group. In brief, immature cumulus–oocyte complexes (COCs) were aspirated from local slaughterhouse-derived ovaries and matured in groups of 50 for 24 h in 500 µL tissue culture medium (TCM) 199 + 10% ($v{\cdot}v^{-1}$) fetal calf serum +10 ng·ml^{-1} epidermal growth factor at 39 °C under 5% CO_2 in air. IVF was subsequently achieved by the co-incubation (39 °C under 5% CO_2 in air) of IVM COCs and 10^6 percoll-separated spermatozoa·ml^{-1} from a single fertility-proven bull (Day 0). Following 20 h post-insemination, presumptive zygotes were isolated, denuded by light vortex, and IVC in groups of 25 in 25 µL synthetic oviduct fluid (SOF) until Day 7.

Animal husbandry and ethics

All animals were kept under identical conditions and fed grass and maize silage supplemented with a standard beef ration. All procedures involving animals were approved by the University College Dublin Animal Research Ethics Committee, and licensed by the Irish Health Products Regulatory Authority, in accordance with the European Union Directive 2010/63/EU on the Protection of Animals Used for Scientific Purposes, and the Republic of Ireland Cruelty to Animals Act of 1876.

Estrous synchronization

The estrous cycles of 28 Charolais-Limousin heifers with a mean age (±SD) of 2.1 ± 0.3 years and weight (±SD) of 606.7 ± 32.0 kg were synchronized with an injection of a gonadotropin releasing hormone (GnRH) analog (Ovarelin; Ceva Santé Animale, Libourne, France) concurrent with the insertion of a progesterone releasing intravaginal device (PRID Delta; Ceva Santé Animale). Seven days later, a prostaglandin F2α (PGF2α) analog (Enzaprost; Ceva Santé Animale) was administered, with PRID removal the next day (Figure 1A). Beginning 30 h following PRID removal, all heifers were observed for signs of estrus five times per day. Day 0 was estimated to be analogous to the day of fertilization—i.e., 28–32 h after first standing heat for mounting [33]. This was to ensure physiological synchrony between in vitro-produced and subsequently transferred embryos (discussed below).

Embryo transfer

On Day 7 post-estrus, ovaries were assessed by transrectal ultrasound. Four heifers lacking an appropriately developed corpus luteum (CL) were excluded. Between 5 and 15 in vitro-produced Day 7 embryos were transferred into the uterine horn ipsilateral to the ovary bearing the CL of the remaining 24 heifers. More specifically, to retrieve sufficient Days 10, 12, 14, and 16 conceptuses, 135, 75, 75, and 20 embryos were transferred into 9, 5, 6, and 4 heifers, respectively (Figure 1A).

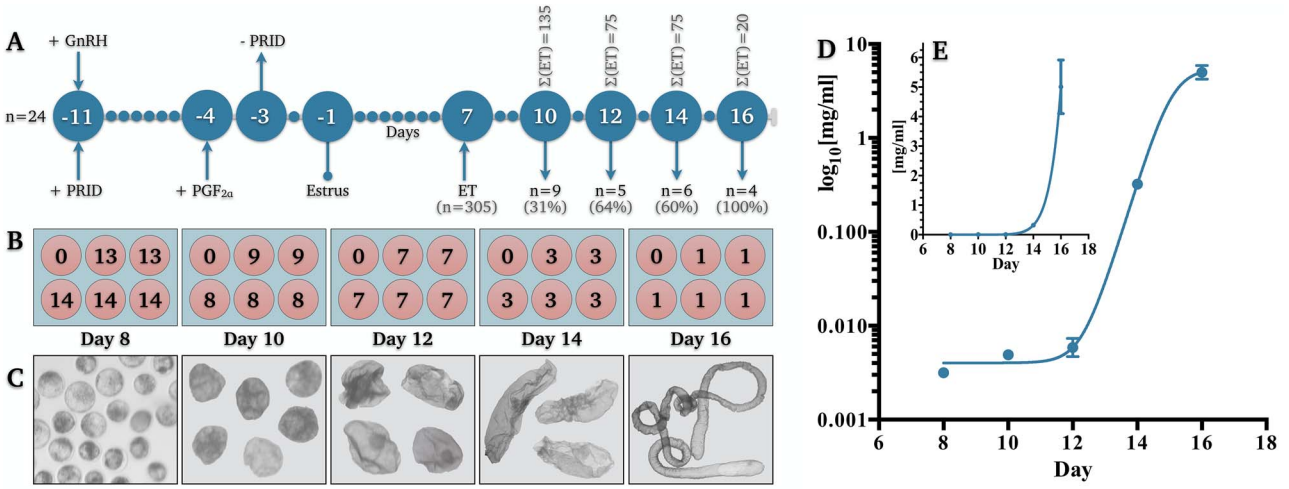

Figure 1. Experimental design and conceptus elongation validation. (A) Schematic depiction of the animal synchronization protocol for embryo and conceptus recovery wherein "Σ(ET)" denotes the total number of embryos transferred per cohort and "*n*" denotes the number of recipient heifers per cohort. Percentages denote the proportion of conceptuses recovered. (B) Diagrammatical representation of embryo and conceptus culture design providing biological ($n = 5$) replicate values per day in addition to the number of conceptuses pooled ($n = 1$–14) per replicate. (C) Representative images of recovered embryos/conceptuses (not to scale). Mean (±SEM) total protein concentration per embryo or conceptus per day on (D) logarithmic and (E) linear axes ($R^2 = 0.976$). Abbreviations: progesterone releasing intra-vaginal device (PRID), gonadotropin releasing hormone (GnRH), and prostaglandin F2 alpha (PGF2α), embryo transfer (ET).

Conceptus recovery and culture

Reproductive tracts were recovered at slaughter and transported to the laboratory within 45 min, where both uterine horns were flushed with 45 mL pre-equilibrated phosphate-buffered saline (PBS). Recovered conceptuses were immediately transferred into serum-free SOF supplemented with 0.1% polyvinyl alcohol (SOFPV). Specifically, conceptuses were cultured in 500 µL SOFPV per well, either singularly (Day 16) or in groups (Days 10–14; Figure 1B), based on consistent morphology (Figure 1C). Conceptuses were cultured at 39 °C in 5% CO_2 in air for 6 h, as was a control SOFPV aliquot devoid of any conceptuses. The same SOFPV batch was used throughout this study to eliminate batch-to-batch composition variability.

Conceptus and conditioned media recovery

Post-culture, conceptuses were isolated, rinsed twice in chilled PBS and snap-frozen in liquid nitrogen, prior to storage at −80 °C until protein content analysis. Specifically, all conceptuses per given well were snap frozen together to determine the conceptus protein content per well for normalization (discussed below). In parallel, conceptus-conditioned and SOFPV control media were centrifuged at 1000 *x g* for 15 min at 4 °C before supernatant snap-freezing in liquid nitrogen and storage at −80 °C until metabolomic analysis.

Conceptus analysis: total protein quantification

Each vial comprising recovered conceptuses was thawed on ice and centrifuged at 16 100 *x g* for 20 min. The supernatant was discarded, and the resulting pellet was lysed with an aqueous buffer comprising 150 mM NaCl + 10 mM tris-hydroxymethyl-aminomethane (THAM) + 1 mM ethylenediaminetetraacetic acid (EDTA) + 1 mM egtazic acid (EGTA) + 1% octylphenoxypolyethoxyethanol (Igepal) + 1 mM phenylmethanesulfonyl fluoride (PMSF) + 2.5 mM Na_3VO_4 + phosphatase cocktail inhibitor and protease cocktail inhibitor at pH 7.4 identically to Aburima et al. [34]. Total protein in each lysed sample was subsequently determined against a standard curve using the DC (calorimetric) protein assay kit (Bio-Rad)—based on the Lowry method [35]—coupled to a microplate reader (Infinite 200 Pro, Tecan) ($\lambda = 750$ nm) in accordance with the manufacturer's instructions.

Conditioned media analysis: mass spectroscopy

Experimental and SOFPV control samples were screened for metabolites by ultrahigh-performance liquid chromatography tandem mass spectroscopy (UPLC-MS/MS) by Metabolon Inc. as described below.

Protein was precipitated and extracted using the automated MicroLab STAR system (Hamilton Company) with methanol under vigorous centrifugation at 680 *x g* for 2 min (Geno/Grinder 2000, Glen Mills) prior to methanol removal using a TurboVap (Zymark) and overnight incubation in nitrogen. Each sample was subsequently divided into four fractions—two for analysis by reverse phase (RP) UPLC-MS/MS with positive ion mode electrospray ionization (ESI), one for analysis by RP UPLC-MS/MS with negative ion mode ESI, and one for analysis by hydrophilic interaction liquid chromatography (HILIC) UPLC-MS/MS with negative ion mode ESI.

Sample extracts were then dried and reconstituted in solvents compatible to each UPLC-MS/MS procedure. Specifically, the first fraction analyzed under positive ionization was subject to gradient elution (Waters UPLC BEH 1.7 µm C18 column 2.1 x 100 mm) in water and methanol with 0.05% perfluoropentanoic acid and 0.1% formic acid. The second run under positive ESI was identically eluted, using the same column, but with the elution buffer additionally comprising acetonitrile. The third fraction, analyzed under negative ionization, was similarly eluted using a gradient buffer comprising methanol, water, and 6.5 mM ammonium bicarbonate (pH 10.8), and the fourth ran under negative ESI and was eluted using a HILIC (Waters UPLC BEH Amide 1.7 µm column 2.1 x 150 mm) with a water plus acetonitrile plus 10 mM ammonium formate (pH 10.8) gradient.

Samples were subsequently analyzed using a Waters Acquity UPLC coupled to a Thermo Scientific Q-Exactive high resolution MS interfaced with heated electrospray ionization (HES-II) source and Orbitrap mass analyzer operating at 35 000 mass resolution and with a scan range between 70 and 1000 *m/z*. Biochemicals were quantified

against known internal and recovery standards, run in parallel, as described below. Metabolite identification was based on retention time/index (RI), mass to charge ratio (*m/z*) within ±10 ppm, and MS/MS forward and reverse scores between the experimental data vs. Metabolon Inc. in-house authentic standards. In a minority of cases where this was not possible, metabolite identification was predicted by comparing metabolite RI, *m/z*, and chromatographic (MS/MS spectral data) to those of purified standards; predicted metabolites are listed in Figure 5 and Supplementary Table S2. The technical (instrument) median relative standard deviation was 3% with a total process variability of 8%.

Metabolomics quality control

Three controls were analyzed in parallel with the experimental samples, the first being a pooled aliquot of all experimental samples, serving as a technical replicate control. Secondly, ultra-pure water samples served as process blanks, also run in between the experimental samples at defined intervals. Thirdly, a cocktail of quality control (QC) metabolites, absent from endogenous compound measurements, were spiked into each sample. This internal standard enabled instrument performance monitoring and chromatographic alignment.

Biochemical data analysis and data presentation

The raw chromatographic data were logarithmically (ln) transformed (i.e., scaled) with neither imputation nor sample media subtraction. These semi-quantitative data pertinent to metabolite flux in conceptus-conditioned medium (CCM) are presented as either conceptus-normalized (CN)—i.e., on an individual conceptus basis, whereby raw peak area values used to calculate the relative concentration of each metabolite were divided by the number of conceptuses per well (Figure 1B) prior to further processing (i.e., representative of the metabolite concentration to which the endometrium would be exposed in vivo), or protein-normalized (PN)—i.e., on a total protein basis, whereby raw peak area values were divided by the total protein concentration of each well before further processing. The former is reflective of conceptus-mediated extracellular changes (i.e., conceptus being the unit), whereas the latter, as conducted by Morris et al. [28], is indicative of changes in conceptus cell metabolism (i.e., per unit protein). A two-way analysis of variance and Welch's two-sample *t*-test, with a $P \leq 0.05$ denoted as significant and $0.05 < P < 0.10$ denoted as a trend, was subsequently applied, unless otherwise stated. Biochemical networks were visualized within relevant metabolic networks using MetaboLync™ pathway analysis software (portal.metabolon.com). Additional statistics and heat mapping—details of which are provided within corresponding figure legends—were generated using Prism 8 (GraphPad Inc., CA, USA).

Uterine luminal fluid comparisons

To identify uniquely conceptus-derived metabolites, data generated in this study were qualitatively contrasted against our previous analyses of the composition of ULF from cyclic heifers on Days 12, 13, and 14 [24–27]. Across those studies, a total of 233 metabolites were consistently identified in ULF (Figure 2)—regardless of day or heifer treatment. Whilst metabolite concentrations varied by day and treatment, such quantitative data are not repeated here; however, those data are discussed in the context of disentangling the metabolic reciprocity of maternal–conceptus communication.

Results

Experimental design

Mean (±SEM) total protein per culture well (Figure 1B), irrespective of conceptus number, was 0.043 ± 0.002 mg/ml (Day 8), 0.041 ± 0.004 mg/ml (Day 10), 0.041 ± 0.01 mg/ml (Day 12), 0.966 ± 0.12 mg/ml (Day 14), and 5.01 ± 0.91 mg/ml (Day 16).

Conceptus elongation

Mean (±SEM) total protein per conceptus (Figure 1D) increased from 3.0 ± 0.8 µg/ml (Day 8), 4.9 ± 5.2 µg/ml (Day 10), 5.9 ± 1.4 µg/ml (Day 12), 0.3 ± 0.03 mg/ml (Day 14), to 5.0 ± 0.9 mg/ml (Day 16).

Qualitative metabolite presence

The exponential increase in mean conceptus protein content during elongation (Figure 1D) was accompanied by a comparatively modest linear ($R^2 = 0.9$) increase in the total number of metabolites detected in CCM over time—rising from 132 to 140, 148, 237, and 280 on Days 8, 10, 12, 14, and 16, respectively (Figure 2A-E). This corresponds to a rate of 19.7 new metabolites per day. These metabolites clustered within 8 super-pathways; overall super-pathway mean (±SD) distribution in terms of the percentage of total corresponding metabolites in CCM across all days was: amino acids (45.0 ± 4.2%), lipids (20.4 ± 2.7%), nucleotides (9.6 ± 5.3%), xenobiotics (8.2 ± 1.6%), carbohydrates (6.2 ± 1.3%), energy substrates (5.2 ± 0.8%), peptides (3.0 ± 1.9%), and cofactors and vitamins (2.2 ± 0.8%) (Figure 2A-E). As such, changes in the proportions of each super-pathway by day were relatively subtle. The unconditioned (SOF control) medium comprised 98 metabolites, spanning the same 8 super-pathways in similar proportions (Figure 2F).

Contrasting CCM and SOF by day revealed 37, 43, 53, 140, and 182 conceptus-secreted metabolites on Days 8–16 (Figure 2A-E). Intriguingly, further contrasting these data against our previous interrogation of ULF composition (Figure 2G) [26] revealed 90 metabolites unique to CCM, being undetected in blank SOF and ULF (Figure 2E)—i.e., uniquely conceptus-derived. Of these, just 14 were identified on all days studied (Figure 2I). A full list is provided in Supplementary Table S1. Figure 2H depicts the overlap of CCM metabolites by day—118 were common to CCM on all days, whereas 83 were only common to CCM on Days 14 and 16, and 36 metabolites were unique to Day 16 CCM.

Semi-quantitative metabolite flux: conceptus normalized

Principal component analysis of all metabolites, and their relative concentrations in CCM, revealed that conceptus-normalized CCM biochemical profiles were most distinct on Days 14 and 16 (Figure 3A). Total metabolite concentrations in CCM increased on Day 16 alone (Figure 3B). This broad profile was near-identical to the breakdown of just amino acid-related metabolites (Figure 3C). Significant differences in carbohydrate (Figure 3D), cofactor and vitamin (Figure 3E), energy substrate (Figure 3F), nucleotide (Figure 3H), lipid (Figure 3G), peptide (Figure 3I), or xenobiotic (Figure 3J) related metabolites were not observed. Sub-pathway comparisons of relative metabolite concentrations by day (Figure 3K) confirm the negligible differences in metabolite turnover preference by the conceptus until Day 16. However, Figure 3K additionally shows a propensity by the Day 16 conceptus to

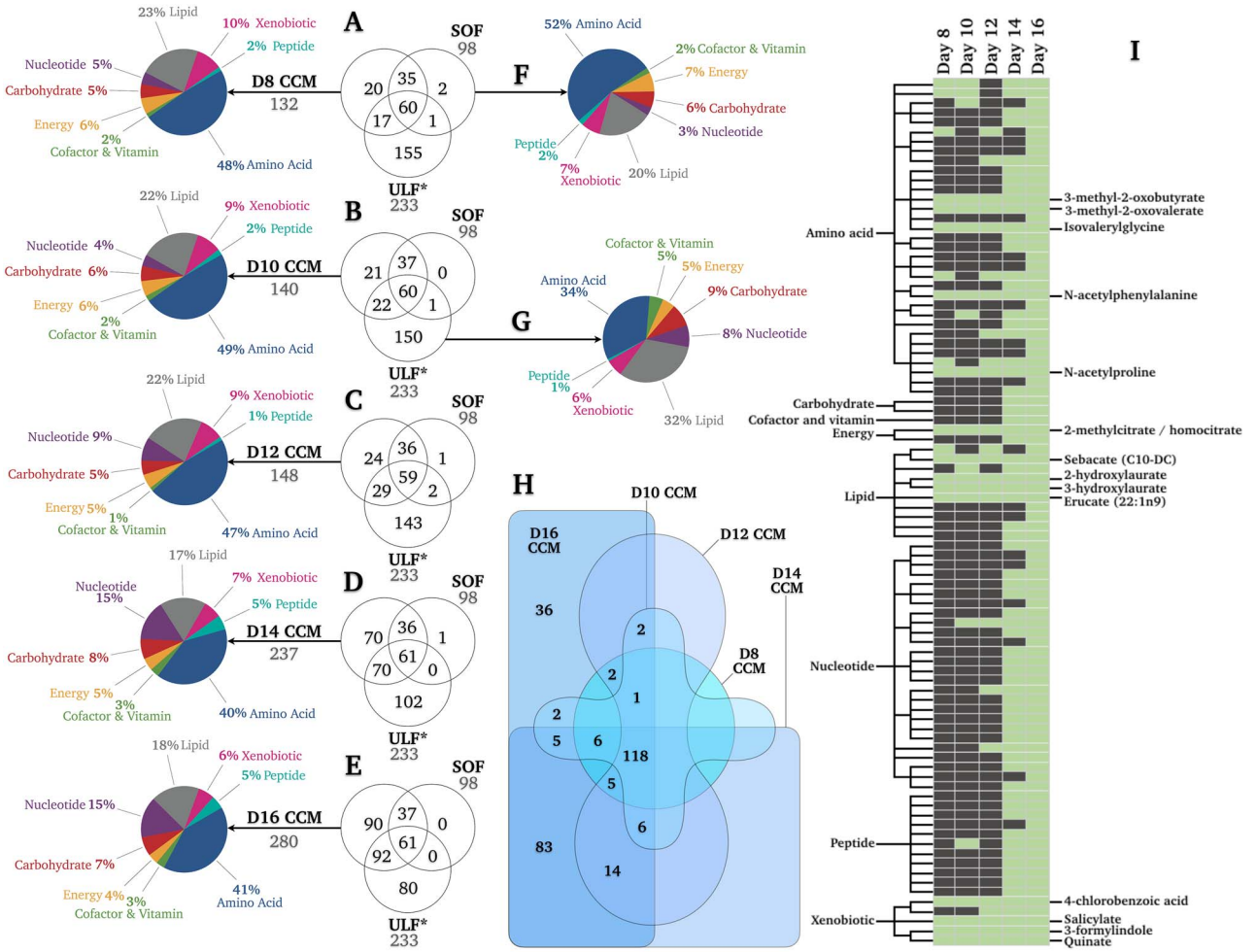

Figure 2. Qualitative metabolomic analyses of conceptus biochemical turnover. (A-E) Venn diagrams depicting the number of metabolites unique and common to Days 8–16 CCM vs. SOF vs. ULF. Asterisks denote data from [24]. Metabolite distributions by super-pathway are also provided for CCM (A-E), SOF (F), and ULF (G) in terms of proportion (%) of total identified metabolites. (H) Number of metabolites unique and common to CCM from Day 8 vs. 10 vs. 12 vs. 14 vs. 16 conceptuses. (I) List of conceptus-derived metabolites (i.e., neither identified in SOF nor ULF) identified in CCM on Days 8, 10, 12, 14, and 16, wherein green and gray indicate present or not detected, respectively. Metabolite names are provided for the 14 metabolites produced by conceptuses on all days studied. Complete datasets are provided as Supplementary Material. Abbreviations: Day 8-16 (D8-16), conceptus-conditioned medium (CCM), synthetic oviduct fluid (SOF), and uterine luminal fluid (ULF).

secrete higher levels of metabolites primarily related to: (a) fructose, mannose, and galactose, (b) creatine, (c) glycolysis, gluconeogenesis, and pyruvate, and (d) (hypo)xanthine/inosine-containing purine metabolism. The complete list of metabolites and their conceptus-normalized fold-changes is provided in Supplementary Table S2.

Regarding conceptus-normalized individual metabolite flux, only two decreases ($P \leq 0.05$) were observed. Firstly, the creatine level declined in CCM on Day 10 vs. 8 by 0.13-fold (Supplementary Table S2). As creatine was not detected in SOF and identified in CCM on Day 10, it was not absorbed, but secreted less on Day 10. Similarly, 2-hydroxylaurate exhibited a 0.61-fold decrease on Day 16 vs. 14 (Supplementary Table S2). This lipid was not identified in SOF, was detected in only one Day 16 CCM replicate, and was present in all five Day 14 replicates. As such, it too was secreted less on Day 16. Moreover, two trends ($0.05 < P < 0.10$) towards a decrease were observed, by cysteine-s-sulfate (0.69-fold; Day 12 vs. 10) and 3-methyl-2-oxovalerate (0.68-fold; Day 10 vs. 8). In contrast, the largest cross-day conceptus-normalized increases ($P \leq 0.05$) observed include: (i) 126 603-fold in xanthine on Day 16 vs. 10, (ii) 37 647-fold in glycerophosphorylcholine (GPC) on Day 16 vs. 8 and 10, (iii) 18 987-fold choline on Day 16 vs. 10, (iv) 14 806-fold in mannitol/sorbitol on Day 16 vs. 8, and (v) 14 073-fold in acetylcarnitine on Day 16 vs. 8 (Supplementary Table S2; Figure 6).

Semi-quantitative metabolite flux: protein normalized

Consistent with conceptus-normalized data, protein-normalized CCM biochemical profiles were most distinct on Days 14 and 16 (Figure 4A). Intriguingly, total metabolic output declined on Day 14 (Figure 4B). Specifically, mean (±SEM) total metabolite flux increased by 1.14 ± 0.03-fold on Day 10 vs. 8 ($n = 125$), 1.80 ± 0.20-fold on Day 12 vs. 10 ($n = 127$), and 2.83 ± 0.42-fold on Day 16 vs. 14 ($n = 237$), but declined by 0.22 ± 0.05-fold on Day 14 *vs.* 12 ($n = 143$). This decline on Day 14 vs. 12 is attributable to the depletion ($P \leq 0.05$) of 85.3% of identified CCM metabolites in the same comparison (Supplementary Table S2). Breaking these data down by super-pathways shows similar profiles across the board (Figure 4C-J). Sub-pathway comparisons of relative metabolite concentrations by day (Figure 4K) confirm the fairly ubiquitous

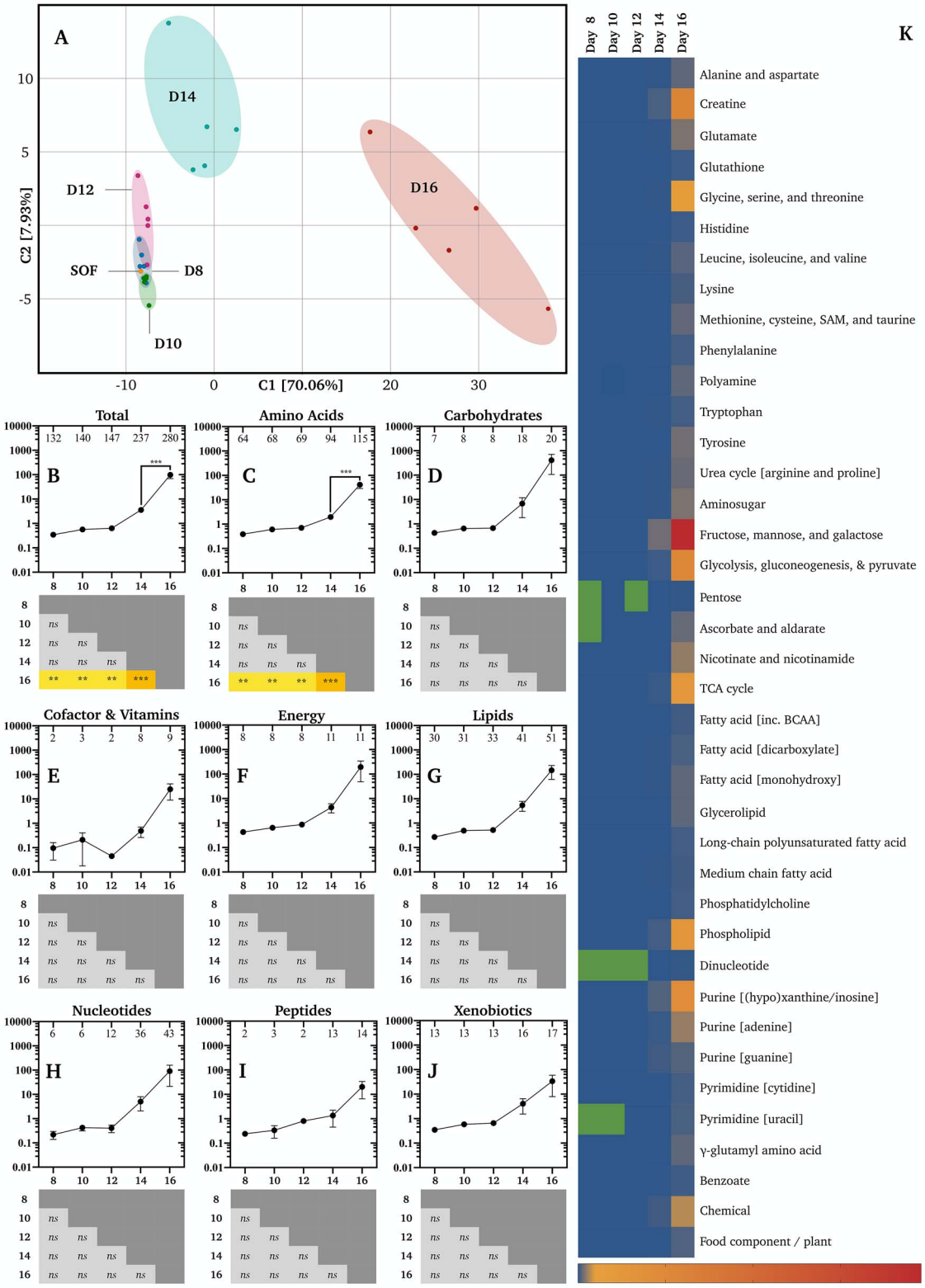

Figure 3. Conceptus-normalized semi-quantitative metabolomics. (A) Principal component analysis of biochemical profiles of synthetic oviduct fluid (SOF) and conceptus conditioned medium (CCM) by developmental stage (Days 8–16). Relative mean (±SEM) concentrations (n = 5 per group) of (B) all metabolites, (C) amino acid, (D) carbohydrate, (E) cofactor and vitamin, (F) energy substrate, (G) lipid, (H) nucleotide, (I) peptide, and (J) xenobiotic related metabolites (vertical axes) by day (horizontal axes). Numbers of identified metabolites within each group are provided within the upper frame of each graph. Differences determined by ordinary one-way analysis of variance coupled to a Tukey non-parametric post hoc test (**** = $P \leq 0.0001$, *** = $P \leq 0.001$, ** = $P \leq 0.01$, and * = $P \leq 0.05$). (K) Heat-maps of metabolite fold-changes about the mean by sub-pathway across days. Green cells denote a lack of identified metabolites, whereas blue to red (bottom-right) denotes the scaled intensity of the change. Additional abbreviations: s-adenosyl methionine (SAM), tricarboxylic acid cycle (TCA), and branch-chain amino acids (BCAA).

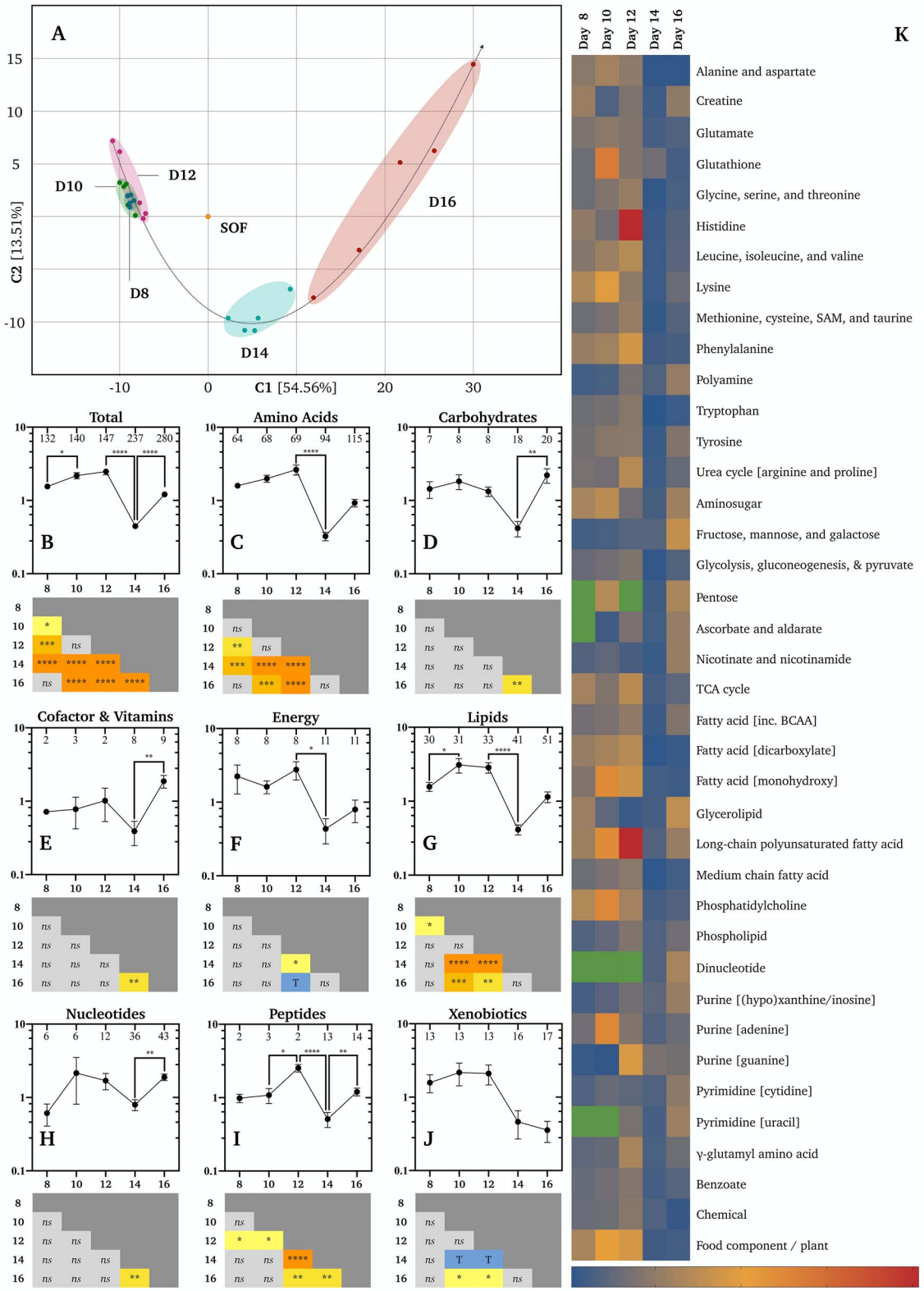

Figure 4. Protein-normalized semi-quantitative metabolomics. (A) Principal component analysis of biochemical profiles of synthetic oviduct fluid (SOF) and conceptus conditioned medium (CCM) by developmental stage (Days 8–16). Relative mean (±SEM) concentrations (n = 5 per group) of (B) all metabolites, (C) amino acid, (D) carbohydrate, (E) cofactor and vitamin, (F) energy substrate, (G) lipid, (H) nucleotide, (I) peptide, and (J) xenobiotic related metabolites (vertical axes) by day (horizontal axes). Numbers of identified metabolites within each group are provided within the upper frame of each graph. Differences determined by ordinary one-way analysis of variance coupled to a Tukey non-parametric post hoc test (**** = $P \leq 0.0001$, *** = $P \leq 0.001$, ** = $P \leq 0.01$, and * = $P \leq 0.05$). (K) Heat-maps of metabolite fold-changes about the mean by sub-pathway across days. Green cells denote a lack of identified metabolites, whereas blue to red (bottom-right) denotes the scaled intensity of the change. Additional abbreviations: s-adenosyl methionine (SAM), tricarboxylic acid cycle (TCA), and branch-chain amino acids (BCAA).

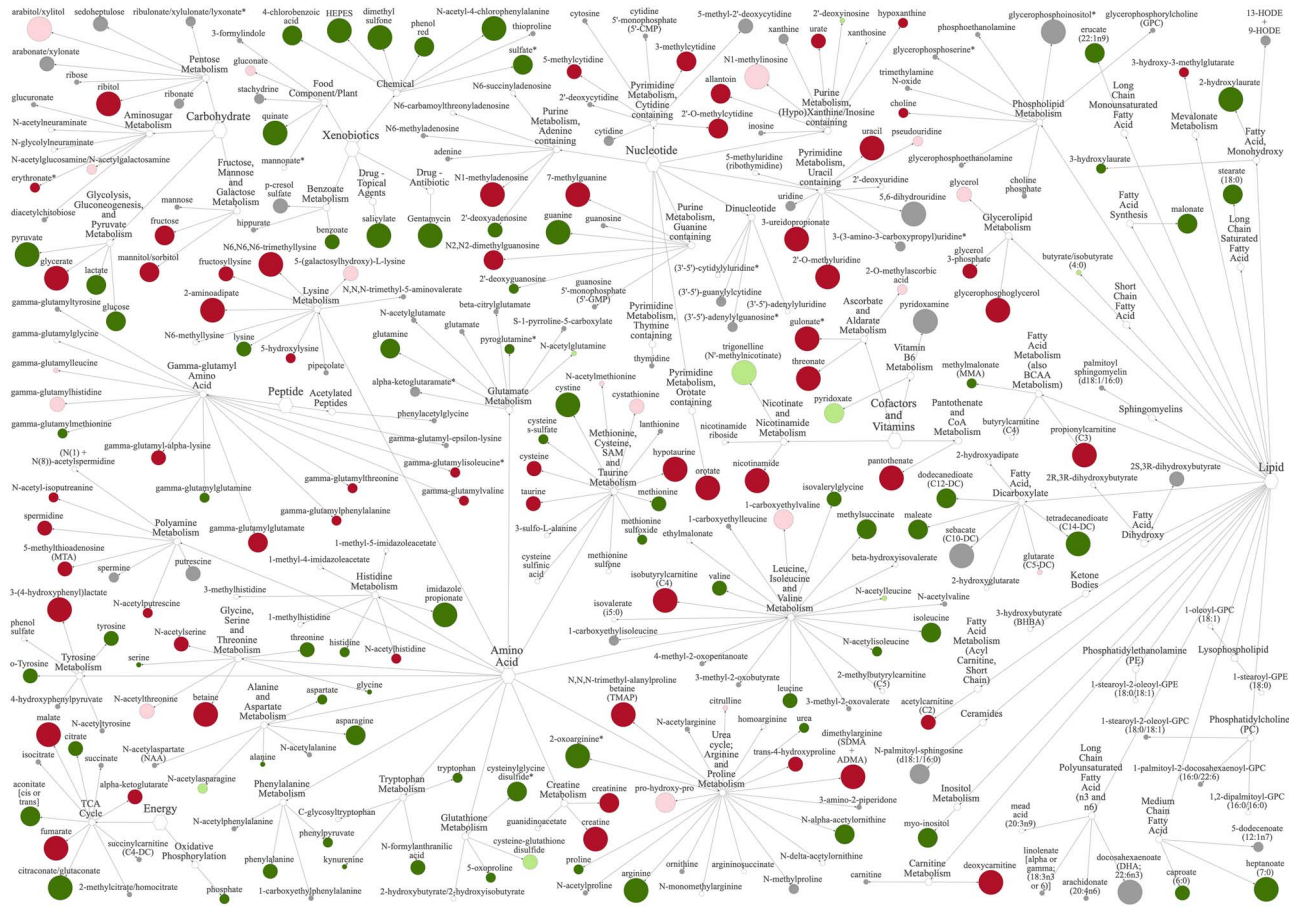

Figure 5. Filamentous vs. tubular conceptus biochemical turnover. Network view of metabolites within corresponding super-pathways and sub-pathways in the conceptus-conditioned media on Day 16 vs. 14 when normalized for total protein. Node diameter and color describe metabolite fold-change magnitude and directionality, respectively: Dark red and dark green respectively indicate an increase or decrease ($P \leq 0.05$), whereas pink or light green denote a trend ($0.05 < P < 0.10$) towards a respective increase or decrease. Gray depicts a lack of a statistically significant difference. Asterisks denote predicted metabolites.

nature of this Day 14 less secretory—or comparatively retentive—phenotype. In contrast, protein-normalized CCM data from Day 16 vs. 14 reveal a reduction ($P \leq 0.05$) of 69 metabolites by a mean (±SEM) of 0.27 ± 0.14-fold, and the parallel elevation ($P \leq 0.05$) of 59 by a mean (±SEM) of 7.22 ± 1.43-fold (Supplementary Table S2; Figure 5).

Regarding such individual metabolite flux in CCM, accounting for protein-normalization, across all comparisons, the largest increases ($P \leq 0.05$) observed include: (i) 81.40-fold in hypotaurine on Day 16 vs. 14, (ii) 67.64-fold in xanthine on Day 16 vs. 8, (iii) 33.71-fold in ribitol on Day 16 vs. 14, (iv) 30.9-fold in GPC on Day 16 vs. 8, (v) 28.59-fold in guanine on Day 12 vs. 8, (vi) 19.66-fold in choline on Day 16 vs. 10, (vii) 15.76-fold in 3-(4-hydroxyphenyl)lactate on Day 16 vs. 14, (viii) 15.71-fold in orotate on Day 16 vs. 14, (ix) 14.08-fold in N6, N6, N6-trimethyllysine on Day 16 vs. 14, and (x) 13.91-fold in spermidine on Day 16 vs. 10. In contrast, over 70 metabolites exhibited a significant ≤ 0.01-fold decrease across all protein-normalized comparisons (Supplementary Table S2).

Discussion

This study provides a detailed characterization of the metabolic fingerprint of the developing bovine embryo in the period from the blastocyst stage to the elongated conceptus at the time of maternal pregnancy recognition. Main findings include: (a) the identification of 14 uniquely conceptus-derived and consistently secreted, as well as other stage specific, metabolites (Figure 2I), (b) an increase in conceptus metabolic output with time (Figure 3B), (c) different metabolite utilization between the spherical (Day 8), tubular (Day 14), and filamentous (Day 16) conceptus (Figures 3 and 4), and (d) on the cellular (protein-normalized) level, the tubular Day 14 conceptus exhibits a metabolically retentive phenotype (Figure 4B and K). Moreover, based on these data and existing literature, a metabolic mechanism underlying maternal–conceptus communication during the conceptus elongation window is presented (Figure 6) and discussed below.

Qualitative metabolomics

The characteristic exponential increase in total conceptus protein content during elongation (Figure 1D) was accompanied by a linear increase in the number of metabolites identified in CCM (Figure 2A-E). Specifically, the scale of conceptus metabolism increased with developmental stage, evidenced by the rate of metabolite output (+19.7 metabolites/day). This rise was greatest between Day 12 and 14 (+44.5 metabolites/day), coinciding with the conceptus transition from an ovoid to tubular structure (Figure 1C). Contrasting the presence of these metabolites in CCM vs. SOF vs. our previous interrogation of ULF composition (from non-pregnant heifers) (Figure 2G) [26] revealed 90 CCM-positive but SOF and

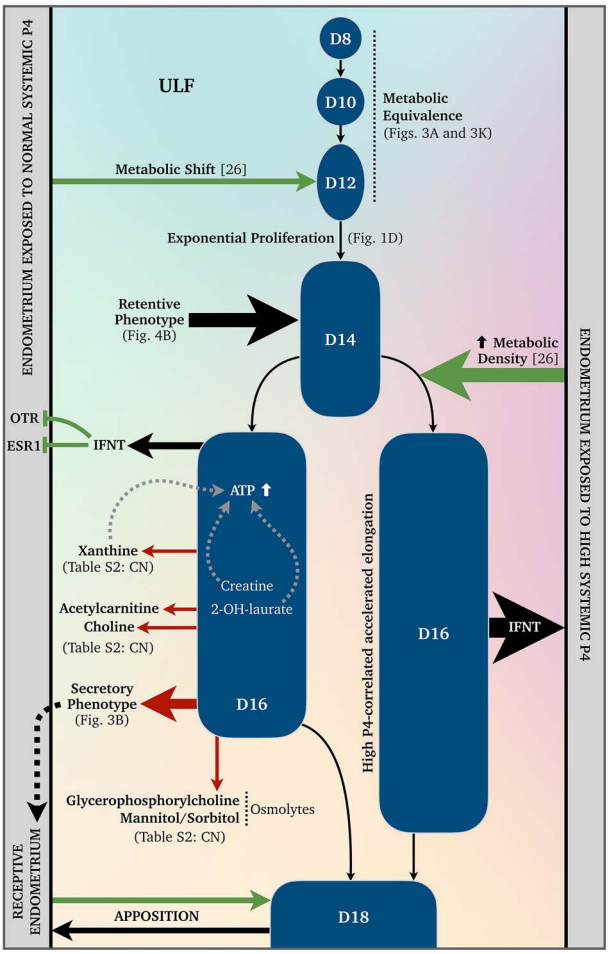

Figure 6. Metabolomic signature of maternal-conceptus communication during conceptus elongation. A schematic depiction of our current understanding of the metabolomics surrounding bovine conceptus elongation. Dashed arrows indicate speculative autocrine and paracrine signaling. Abbreviations: uterine luminal fluid (ULF), Days 8–18 conceptus (D8–D18), oxytocin receptor (OTR), estrogen receptor alpha (ESR1), interferon tau (IFNT), progesterone (P4), and conceptus-normalized (CN).

ULF-negative (i.e. uniquely conceptus-derived) metabolites. It is important to note that failure to detect these metabolites in ULF may be related to a dilution effect and requires validation. Nonetheless, 14 of these 90 conceptus-derived metabolites were detected in CCM at each developmental stage (Figure 2I). Thus, we extrapolate that the uterine luminal microenvironment becomes more metabolically diverse (Figure 2H) as pregnancy progresses.

Semi-quantitative metabolomics: conceptus normalized

Regarding our first hypothesis, that metabolite uptake would increase with time, the exponential increase in conceptus protein content was not accompanied by an equivalent increase in metabolite uptake. On the contrary, the total conceptus-normalized metabolite ratio was consistently >1 and rose over time, resulting in a significant difference on Day 16 (Figure 3B).

Interestingly, one of the 14 consistently secreted uniquely conceptus-derived metabolites—2-hydroxylaurate—was the only metabolite to decline in concentration in CCM on Day 16 vs. 14 (Supplementary Table S2)—i.e., retained more by the Day 16 conceptus. To our knowledge, the only other study linking 2-hydroxylaurate to pregnancy is a recent metabolomic analysis of human placentas from spontaneous preterm (SPTB) vs. physiological births, which identified elevated 2-hydroxylaurate as a marker of SPTB [36].

Creatine similarly bucked the trend, declining in CCM on Day 10 vs. 8 (Supplementary Table S2). A primary function of this non-proteinogenic amino acid is ADP to ATP regeneration in tissues with high and fluctuating energy demands [37]. Moreover, intracellular creatine delays ATP loss under hypoxic–ischemic conditions [38, 39] whilst elevated creatine kinase activity can protect against hypoxia [40]. As such, creatine retention by the conceptus at the onset of elongation may facilitate ATP recycling within the hypoxic uterine luminal microenvironment [41–43]. Whilst bovine conceptus proteomic data are lacking, four subunit isoforms of creatine kinase (CKM, CKB, CKMT1, and CKMT2) have been identified in the murine blastocyst [44]. Similarly, the bovine blastocyst expresses both hypoxia-inducible factors (HIF) 1α and 2α [45], which regulate creatine metabolism [46], and whose knockouts are embryo-lethal in mice [47–49].

The largest cross-day conceptus-normalized increase observed was that of xanthine, whose derivatives are competitive nonselective phosphodiesterase inhibitors [50, 51], between Day 16 vs. 10 (Supplementary Table S2). Given that phosphodiesterase-1β—which catalyzes the conversion of cAMP to AMP [52, 53]—is expressed by the elongating (Days 10–14) porcine conceptus [54], it is tempting to suggest that xanthine secretions are indirect paracrine modulators promoting conceptus ATP retention, in a cooperative manner to that proposed for creatine (Figure 6).

Furthermore, *PPARG*—encoding peroxisome proliferator-activated receptor gamma (PPARγ), a nuclear receptor protein and transcription factor regulating glycolysis—expression is elevated in the bovine conceptus at the onset of elongation [55], as is *PRKAB2*—encoding the AMPK regulatory subunit, which senses ADP/ATP status and glucose availability [19, 56]. These data, combined, suggest that intra-conceptus ATP generation and retention are fundamental traits of bovine conceptus-associated membrane elongation.

Regarding the second hypothesis, that metabolite consumption would correlate to previously identified uterine secretions, the broad biochemical turnover in CCM on Days 12 and 14 mapped fairly well with previously studied uterine secretions [24–27]. Specifically, of the 62 depleted metabolites in ULF on Day 14 vs. 12 [26], 52 were identified in CCM, of which 37 were elevated in the conceptus-normalized CCM on Day 14 vs. 12. This inversely proportional metabolite flux between ULF and CCM strongly supports the notion of a significant metabolic component to conceptus–maternal interactions during the conceptus elongation window. Concerning our third hypothesis, that metabolite utilization would differ between the spherical vs. filamentous conceptus, this was indeed the case within both a conceptus- (Figure 3A) and protein-normalized (Figure 4A) contexts, as demonstrated by the clear group separation of Days 8 and 16 profiles by principal component and network (Supplementary Figure S1) analyses.

Semi-quantitative metabolomics: protein normalized

To our knowledge, only one study has investigated ruminant conceptus metabolite consumption and release; Morris et al. [28] quantified the turnover of 18 amino acids (protein-normalized) by Days 14–16 bovine conceptuses cultured in vitro for either 1, 4,

or 8 h. Arginine was consistently depleted, whereas alanine and glutamate were consistently produced, during all culture durations. Arginine was consistently consumed in this study too (Supplementary Table S2)—perhaps unsurprising given that arginine in part stimulates ovine trophectoderm migration and adhesion [57], improves porcine reproductive performance following dietary supplementation [58], is a placental nitric oxide and polyamine source [59], and regulates conceptus gene expression [59–61].

In contrast, alanine and glutamate were not released by conceptuses on Day 14 vs. 12 and 16 vs. 14 here. However, one key difference between this study and that by Morris *et al*. [28] is their use of in vivo-derived conceptuses. Given that the in vivo Day 20 [62] and in vitro Day 15 [63] endometrial transcriptome differs in the presence of in vivo vs. in vitro derived conceptuses, it seems reasonable to assume that these differences may be attributable to differential metabolism by in vivo vs. in vitro derived conceptuses.

Moreover, it is worth noting that the conceptus incubation duration of 6 h was selected based on previous work by Morris et al. [28], who observed accelerated amino acid depletion by conceptuses during 1 h vs. 4 and 8 h culture, speculating that the latter turnover rates are more likely to reflect a steady state, and Forde et al. [64], who noted negligible differences in the protein secretome of Day 16 bovine conceptuses cultured for 6 vs. 24 h.

Morris et al. [28] also observed that the broad pattern of amino acid turnover by the elongating conceptus was similar to that of the early (Days 1–7) embryo. However, this, coupled with reduced de novo protein synthesis during elongation [65] suggests that metabolite utilization differs between the spherical vs. filamentous conceptus, as confirmed by Figures 3 and 4.

Lastly, a significant decline in metabolic output by the tubular Day 14 conceptus was observed when the data were normalized for protein (Figure 4B). Specifically, the increased mean (±SEM) conceptus protein content (Figure 1E) on Day 14 (0.32 ± 0.03 mg/ml) vs. 12 (0.006 ± 0.0001 mg/ml) was not accompanied by a similarly elevated metabolic output, as the mean (±SEM) non-normalized metabolite fold change on Day 14 vs. 12 was 6.13 ± 1.1-fold. The protein-normalized decline in secretions on Day 14 vs. 12 was, therefore, 0.23 ± 0.05-fold, and, as such, was comparatively absorptive. However, given that the Day 14 CCM vs. SOF metabolite ratio did not fall below 1, we refer to this phenotype as retentive.

These data in the context of existing literature, point towards a mechanism underpinning accelerated conceptus elongation following elevated systemic P4 [23] as the metabolically retentive phenotype of the Day 14 conceptus (Figure 4B) coincides with high P4-induced (i) advanced endometrial gene expression [66] and (ii) a more metabolically dense ULF [26]—both on Day 14 (Figure 6). Thus, it is likely that the metabolic shift observed in the ULF of normal P4 cyclic heifers on Day 12 [26] primes the retentive Days 13–14 conceptus for filamentous trophectoderm proliferation prior to maternal pregnancy recognition around Day 16. This also implies that unsuccessful attempts to recapitulate conceptus elongation in vitro [13–15] may be at least partly attributable to culture media inadequately mimicking sequential composition changes observed in vivo.

Future work

In addition to identifying the aetiologies of differential metabolism by in vivo vs. in vitro derived conceptuses, elucidating whether optimal conceptus development is achieved in an extracellular milieu favoring a "quiet metabolism"—as seems to be the case for the early embryo [67, 68]—is an important area for further research. Additional areas include confirming that the conceptus-derived metabolites identified in this study are unique to the conceptus, i.e., not lost in ULF analyses by dilution, in addition to probing whether the high incidence of metabolite methylation, N-acetylation, and γ-glutamylation among the conceptus-derived metabolites (Supplementary Table S1) is coincidental. Lastly, ex situ conceptus culture in the presence and absence of oxidative phosphorylation inhibitors under advanced oxygen sensing platforms [69] will further enhance our understanding of the biochemistry underpinning conceptus elongation.

Conflict of interest

The authors have declared that no conflict of interest exists.

Author contributions

CAS and PL conceived the idea. CAS, JMS, and PL designed the experiments. CAS, JMS, EOC, MM, and AAA performed the research. CAS and PL analyzed the data, prepared the manuscript, with support from JMS, and acquired funding.

Acknowledgements

Authors thank the staff at Moyvalley Meats and The Kildare Chilling Company, in addition to Drs Greg Palczewski, Pawel Gardzielewski, Edward Karoly, and Brian Ingram at Metabolon Inc., and the students and staff at University College Dublin for their assistance, notably, Mr Stephen Lott, Ms Niamh Cantwell, and Mrs Mary Wade.

Supplementary material

Supplementary material is available at *BIOLRE* online.

References

1. Brooks K, Burns G, Spencer TE. Conceptus elongation in ruminants: roles of progesterone, prostaglandin, interferon tau and cortisol. *J Anim Sci Biotechnol* 2014; **5**:1–12.
2. Betteridge K, Eaglesome M, Randall G, Mitchell D. Collection, description and transfer of embryos from cattle 10-16 days after oestrus. *J Reprod Fertil* 1980; **59**:205–216.
3. Hue I, Degrelle SA, Turenne N. Conceptus elongation in cattle: genes, models and questions. *Anim Reprod Sci* 2012; **134**:19–28.
4. Wales RG, Cuneo CL. Morphology and chemical analysis of the sheep conceptus from the 13th to the 19th day of pregnancy. *Reprod Fertil Dev* 1989; **1**:31–39.
5. Wang J, Guillomot M, Hue I. Cellular organization of the trophoblastic epithelium in elongating conceptuses of ruminants. *C R Biol* 2009; **332**:986–997.
6. Bazer FW, Thatcher WW. Chronicling the discovery of interferon tau. *Reproduction* 2017; **154**:F11–F20.
7. Roberts RM. 30 years on from the molecular cloning of interferon-tau. *Reproduction* 2017; **154**:E1–E2.
8. Kerbler TL, Buhr MM, Jordan LT, Leslie KE, Walton JS. Relationship between maternal plasma progesterone concentration and interferon-tau synthesis by the conceptus in cattle. *Theriogenology* 1997; **47**:703–714.
9. Forde N, Lonergan P. Interferon-tau and fertility in ruminants. *Reproduction* 2017; **154**:F33–F43.
10. Sánchez JM, Mathew DJ, Behura SK, Passaro C, Charpigny G, Butler ST, Spencer TE, Lonergan P. Bovine endometrium responds differentially to age-matched short and long conceptuses. *Biol Reprod* 2019; **101**:26–39.

11. Imakawa K, Bai R, Fujiwara H, Kusama K. Conceptus implantation and placentation: molecules related to epithelial–mesenchymal transition, lymphocyte homing, endogenous retroviruses, and exosomes. *Reprod Med Biol* 2016; **15**:1–11.
12. Ferré LB, Kjelland ME, Strøbech LB, Hyttel P, Mermillod P, Ross PJ. Review: Recent advances in bovine in vitro embryo production: reproductive biotechnology history and methods. *Animal* 2020; **14**:991–1004.
13. Brandão DO, Maddox-Hyttel P, Løvendahl P, Rumpf R, Stringfellow D, Callesen H. Post hatching development: a novel system for extended in vitro culture of bovine embryos. *Biol Reprod* 2004; **71**:2048–2055.
14. Zhao S, Liu ZX, Gao H, Wu Y, Fang Y, Wu SS, Li MJ, Bai JH, Liu Y, Evans A, Zeng SM. A three-dimensional culture system using alginate hydrogel prolongs hatched cattle embryo development in vitro. *Theriogenology* 2015; **84**:184–192.
15. Vajta G, Alexopoulos NI, Callesen H. Rapid growth and elongation of bovine blastocysts in vitro in a three-dimensional gel system. *Theriogenology* 2004; **62**:1253–1263.
16. Isaac E, Pfeffer PL. Growing cattle embryos beyond day 8 - an investigation of media components. *Theriogenology* 2020; **161**:273–284.
17. Ramos-Ibeas P, Lamas-Toranzo I, Martínez-Moro Á, de Frutos C, Quiroga AC, Zurita E, Bermejo-Álvarez P. Embryonic disc formation following post-hatching bovine embryo development in vitro. *Reproduction* 2020; **160**:579–589.
18. Degrelle SA, Campion E, Cabau C, Piumi F, Reinaud P, Richard C, Renard JP, Hue I. Molecular evidence for a critical period in mural trophoblast development in bovine blastocysts. *Dev Biol* 2005; **288**:448–460.
19. Mamo S, Mehta JP, McGettigan P, Fair T, Spencer TE, Bazer FW, Lonergan P. RNA sequencing reveals novel gene clusters in bovine conceptuses associated with maternal recognition of pregnancy and implantation. *Biol Reprod* 2011; **85**:1143–1151.
20. Ribeiro ES, Greco LF, Bisinotto RS, Lima FS, Thatcher WW, Santos JE. Biology of preimplantation conceptus at the onset of elongation in dairy cows. *Biol Reprod* 2016; **94**:1–18.
21. Barnwell CV, Farin PW, Ashwell CM, Farmer WT, Galphin SP, Farin CE. Differences in mRNA populations of short and long bovine conceptuses on day 15 of gestation. *Mol Reprod Dev* 2016; **83**:424–441.
22. Gray CA, Taylor KM, Ramsey WS, Hill JR, Bazer FW, Bartol FF, Spencer TE. Endometrial glands are required for preimplantation conceptus elongation and survival. *Biol Reprod* 2001; **64**:1608–1613.
23. Clemente M, De La Fuente J, Fair T, Al Naib A, Gutierrez-Adan A, Roche JF, Rizos D, Lonergan P. Progesterone and conceptus elongation in cattle: a direct effect on the embryo or an indirect effect via the endometrium? *Reproduction* 2009; **138**:507–517.
24. Simintiras CA, Sánchez JM, McDonald M, Martins T, Binelli M, Lonergan P. Biochemical characterization of progesterone-induced alterations in bovine uterine fluid amino acid and carbohydrate composition during the conceptus elongation window. *Biol Reprod* 2019; **100**:672–685.
25. Simintiras CA, Sánchez JM, McDonald M, Lonergan P. Progesterone alters the bovine uterine fluid lipidome during the period of elongation. *Reproduction* 2019; **157**:399–411.
26. Simintiras CA, Sánchez JM, McDonald M, Lonergan P. The biochemistry surrounding bovine conceptus elongation. *Biol Reprod* 2019; **101**:328–337.
27. Simintiras CA, Sánchez JM, McDonald M, Lonergan P. The influence of progesterone on bovine uterine fluid energy, nucleotide, vitamin, cofactor, and xenobiotic composition during the conceptus elongation-initiation window. *Sci Rep* 2019; **9**:7716.
28. Morris DG, Humpherson PG, Leese HJ, Sreenan JM. Amino acid turnover by elongating cattle blastocysts recovered on days 14-16 after insemination. *Reproduction* 2002; **124**:667–673.
29. Diskin MG, Sreenan JM. Fertilization and embryonic mortality rates in beef heifers after artificial insemination. *J Reprod Fertil* 1980; **59**:463–468.
30. Walsh SW, Williams EJ, Evans ACO. A review of the causes of poor fertility in high milk producing dairy cows. *Anim Reprod Sci* 2011; **123**:127–138.
31. Wiltbank MC, Baez GM, Garcia-Guerra A, Toledo MZ, Monteiro PLJ, Melo LF, Ochoa JC, Santos JEP, Sartori R. Pivotal periods for pregnancy loss during the first trimester of gestation in lactating dairy cows. *Theriogenology* 2016; **86**:239–253.
32. Ribeiro ES, Gomes G, Greco LF, Cerri RLA, Vieira-Neto A, Monteiro PLJ, Lima FS, Bisinotto RS, Thatcher WW, Santos JEP. Carryover effect of postpartum inflammatory diseases on developmental biology and fertility in lactating dairy cows. *J Dairy Sci* 2016; **99**:2201–2220.
33. Walker W, Nebel R, McGilliard M. Time of ovulation relative to mounting activity in dairy cattle. *J Dairy Sci* 1996; **79**:1555–1561.
34. Aburima A, Wraith KS, Raslan Z, Law R, Magwenzi S, Naseem KM. CAMP signaling regulates platelet myosin light chain (MLC) phosphorylation and shape change through targeting the RhoA-rho kinase-MLC phosphatase signaling pathway. *Blood* 2013; **122**:3533–3545.
35. Lowry OH, Rosebrough NJ, Farr AL, Randall RJ. Protein measurement with the folin phenol reagent. *J Biol Chem* 1951; **193**:265–275.
36. Elshenawy S, Pinney SE, Stuart T, Doulias PT, Zura G, Parry S, Elovitz MA, Bennett MJ, Bansal A, Strauss JF, Ischiropoulos H, Simmons RA. The metabolomic signature of the placenta in spontaneous preterm birth. *Int J Mol Sci* 2020; **21**:1–20.
37. Dickinson H, Bain E, Wilkinson D, Middleton P, Crowther CA, Walker DW. Creatine for women in pregnancy for neuroprotection of the fetus. *Cochrane Database Syst Rev* 2014; CD010846 1–2.
38. Baharom S, De Matteo R, Ellery S, Della Gatta P, Bruce CR, Kowalski GM, Hale N, Dickinson H, Harding R, Walker D, Snow RJ. Does maternal-fetal transfer of creatine occur in pregnant sheep? *Am J Physiol Endocrinol Metab* 2017; **313**:E75–E83.
39. Yoneda K, Arakawa T, Asaoka Y, Fukuoka Y, Kinugasa K, Takimoto K, Okada Y. Effects of accumulation of phosphocreatine on utilization and restoration of high-energy phosphates during anoxia and recovery in thin hippocampal slices from the Guinea pig. *Exp Neurol* 1983; **82**:215–222.
40. Zervou S, Whittington HJ, Ostrowski PJ, Cao F, Tyler J, Lake HA, Neubauer S, Lygate CA. Increasing creatine kinase activity protects against hypoxia/reoxygenation injury but not against anthracycline toxicity in vitro. *PLoS One* 2017; **12**:e0182994.
41. Neupane M, Geary TW, Kiser JN, Burns GW, Hansen PJ, Spencer TE, Neibergs HL. Loci and pathways associated with uterine capacity for pregnancy and fertility in beef cattle. *PLoS One* 2017; **12**:e0188997.
42. Dunwoodie SL. The role of hypoxia in development of the mammalian embryo. *Dev Cell* 2009; **17**:755–773.
43. Simon MC, Keith B. The role of oxygen availability in embryonic development and stem cell function. *Nat Rev Mol Cell Biol* 2008; **9**:285–296.
44. Forsey KE, Ellis PJ, Sargent CA, Sturmey RG, Leese HJ. Expression and localization of creatine kinase in the preimplantation embryo. *Mol Reprod Dev* 2013; **80**:185–192.
45. Harvey AJ, Kind KL, Pantaleon M, Armstrong DT, Thompson JG. Oxygen-regulated gene expression in bovine blastocysts. *Biol Reprod* 2004; **71**:1108–1119.
46. Glover LE, Bowers BE, Saeedi B, Ehrentraut SF, Campbell EL, Bayless AJ, Dobrinskikh E, Kendrick AA, Kelly CJ, Burgess A, Miller L, Kominsky DJ, et al. Control of creatine metabolism by HIF is an endogenous mechanism of barrier regulation in colitis. *Proc Natl Acad Sci U S A* 2013; **110**:19820–19825.
47. Peng J, Zhang L, Drysdale L, Fong GH. The transcription factor EPAS-1/hypoxia-inducible factor 2alpha plays an important role in vascular remodeling. *Proc Natl Acad Sci U S A* 2000; **97**:8386–8391.
48. Iyer NV, Kotch LE, Agani F, Leung SW, Laughner E, Wenger RH, Gassmann M, Gearhart JD, Lawler AM, Yu AY, Semenza GL. Cellular and developmental control of O2 homeostasis by hypoxia-inducible factor 1 alpha. *Genes Dev* 1998; **12**:149–162.
49. Ryan HE, Lo J, Johnson RS. HIF-1 alpha is required for solid tumor formation and embryonic vascularization. *EMBO J* 1998; **17**:3005–3015.
50. Singh N, Shreshtha AK, Thakur MS, Patra S. Xanthine scaffold: scope and potential in drug development. *Heliyon* 2018; **4**:e00829–e00829.
51. Boswell-Smith V, Spina D, Page CP. Phosphodiesterase inhibitors. *Br J Pharmacol* 2006; **147**:S252–S257.

52. Bender AT, Beavo JA. Cyclic nucleotide phosphodiesterases: molecular regulation to clinical use. *Pharmacol Rev* 2006; **58**:488–520.
53. Lugnier C. Cyclic nucleotide phosphodiesterase (PDE) superfamily: a new target for the development of specific therapeutic agents. *Pharmacol Ther* 2006; **109**:366–398.
54. Ross JW, Ashworth MD, Stein DR, Couture OP, Tuggle CK, Geisert RD. Identification of differential gene expression during porcine conceptus rapid trophoblastic elongation and attachment to uterine luminal epithelium. *Physiol Genomics* 2009; **36**:140–148.
55. Ribeiro ES, Santos JEP, Thatcher WW. Role of lipids on elongation of the preimplantation conceptus in ruminants. *Reproduction* 2016; **152**:R115–R126.
56. Lin SC, Hardie DG. AMPK: sensing glucose as well as cellular energy status. *Cell Metab* 2018; **27**:299–313.
57. Wang X, Johnson GA, Burghardt RC, Wu G, Bazer FW. Uterine histotroph and conceptus development. II. Arginine and secreted phosphoprotein 1 cooperatively stimulate migration and adhesion of ovine trophectoderm cells via focal adhesion-MTORC2 mediated cytoskeleton reorganization. *Biol Reprod* 2016; **95**:71–71.
58. Mateo RD, Wu G, Bazer FW, Park JC, Shinzato I, Kim SW. Dietary l-arginine supplementation enhances the reproductive performance of gilts. *J Nutr* 2007; **137**:652–656.
59. Bazer FW, Wang X, Johnson GA, Wu G. Select nutrients and their effects on conceptus development in mammals. *Anim Nutr* 2015; **1**:85–95.
60. Kim E. Mechanisms of amino acid sensing in mTOR signaling pathway. *Nutr Res Pract* 2009; **3**:64.
61. Kim J, Song G, Wu G, Gao H, Johnson GA, Bazer FW. Arginine, leucine, and glutamine stimulate proliferation of porcine trophectoderm cells through the MTOR-RPS6K-RPS6-EIF4EBP1 signal transduction pathway. *Biol Reprod* 2013; **88**:1–9.
62. Mansouri-Attia N, Sandra O, Aubert J, Degrelle S, Everts RE, Giraud-Delville C, Heyman Y, Galio L, Hue I, Yang X, Tian XC, Lewin HA, et al. Endometrium as an early sensor of in vitro embryo manipulation technologies. *Proc Natl Acad Sci U S A* 2009; **106**:5687–5692.
63. Mathew DJ, Sánchez JM, Passaro C, Charpigny G, Behura SK, Spencer TE, Lonergan P. Interferon tau-dependent and independent effects of the bovine conceptus on the endometrial transcriptome. *Biol Reprod* 2019; **100**:365–380.
64. Forde N, Bazer FW, Spencer TE, Lonergan P. Conceptualizing' the endometrium: identification of conceptus-derived proteins during early pregnancy in Cattle1. *Biol Reprod* 2015; **92**:1–13.
65. Morris DG, Diskin MG, Sreenan JM. Protein synthesis and phosphorylation by elongating 13-15-day-old cattle blastocysts. *Reprod Fertil Dev* 2000; **12**:39–44.
66. Forde N, Carter F, Fair T, Crowe MA, Evans ACO, Spencer TE, Bazer FW, McBride R, Boland MP, O'Gaora P, Lonergan P, Roche JF. Progesterone-regulated changes in endometrial gene expression contribute to advanced conceptus development in cattle. *Biol Reprod* 2009; **81**:784–794.
67. Baumann CG, Morris DG, Sreenan JM, Leese HJ. The quiet embryo hypothesis: Molecular characteristics favoring viability. *Mol Reprod Dev* 2007; **74**:1345–1353.
68. Steeves TE, Gardner DK. Temporal and differential effects of amino acids on bovine embryo development in culture. *Biol Reprod* 1999; **61**:731–740.
69. Obeidat Y, Catandi G, Carnevale E, Chicco AJ, DeMann A, Field S, Chen T. A multi-sensor system for measuring bovine embryo metabolism. *Biosens Bioelectron* 2019; **126**:615–623.